ELSEVIER

Contents lists available at ScienceDirect

Physics of the Dark Universe

journal homepage: www.elsevier.com/locate/dark



Full Length Article

Variations in Ionospheric Total Electron Content and Scintillation at GPS stations in Uzbekistan and China during the Annular Solar Eclipse on June 21, 2020

H.E. Eshkuvatov ^{a,b,c,*}, Punyawi Jamjareegulgarn ^e, B.J. Ahmedov ^{a,c,d}, Y.A. Tillayev ^c, Z.J. Ruziev ^b, E.Zh. Kosbergenov ^b, N.Q. Abdullayev ^b, Libo Liu ^{f,g,h}, Sh.A. Sayfulloyev ^b, M.A. Musurmonov ⁱ

- ^a Institute for Advanced Studies, New Uzbekistan University, Movarounnahr str. 1, Tashkent 100000, Uzbekistan
- ^b National University of Uzbekistan, Faculty of Physics, University Street 4, Tashkent 100095, Uzbekistan
- ^c Ulugh Beg Astronomical Institute, Astronomy St. 33, Tashkent 100052, Uzbekistan
- ^d Institute of Theoretical Physics, National University of Uzbekistan, Tashkent 100174, Uzbekistan
- e King Mongkut's Institute of Technology Ladkrabang, Prince of Chumphon Campus, Chumphon, 86160, Thailand
- f Key Laboratory of Earth and Planetary Physics, Institute of Geology and Geophysics, Chinese Academy of Sciences, Beijing, China
- g College of Earth and Planetary Sciences, University of Chinese Academy of Sciences, Beijing, China
- h Heilongjiang Mohe National Observatory of Geophysics, Institute of Geology and Geophysics, Chinese Academy of Sciences, Beijing, China
- ⁱ Kimyo International University in Tashkent, Shota Rustaveli street, 156, 100121 Tashkent, Uzbekistan

ARTICLE INFO

Keywords: Ionosphere Solar eclipse GNSS GPS TEC Scintillation

ABSTRACT

This study presents a novel investigation into the distinct ionospheric variations observed over China and Uzbekistan during the annular solar eclipse on June 21, 2020. For the first time, we demonstrate the influence of this celestial event on Total Electron Content (TEC) measurements obtained from GPS satellites. We analyzed fluctuations in TEC and the Ionospheric Scintillation Index (S4) across six strategically selected sites—three in Uzbekistan (MTAL, KIT3, MADK) and three in China (JFNG, LHAZ, BJFS) located near the eclipse path, with obscuration levels of 52%, 57%, 58%, in Uzbekistan and 92%, 94% and 95% in China. Our study involved continuous monitoring of ionospheric parameters over three days, from June 20 to June 22, 2020. Results indicated a significant TEC depletion ranging from 10% to 30% on the day of the eclipse. The analysis reveals that both TEC levels and the S4 scintillation index experienced notable reductions during the event, attributed to the decreased ionizing radiation. These findings enhance our understanding of ionospheric dynamics in response to solar eclipses and have important implications for satellite communication and navigation systems.

1. Introduction

Similar studies have previously been examined by [1–5], and [6]. We express our deepest gratitude for these contributions. One of the most significant topics extensively investigated in the literature is the impact of solar eclipses on key ionospheric parameters (see, e.g., [7–10]).

During a solar eclipse, the ionosphere is affected due to the complete or partial obstruction of solar radiation. This results in a decrease in the number of electrons and ions in the ionosphere's F-layer. Various factors, including the degree of solar and geomagnetic disturbances, latitude, longitude, and local time, contribute to disturbances in the F-layer. During a solar eclipse, these factors cause a decrease in ionization in the F-region of the ionosphere, where dynamic processes play a

crucial role. Over the past years, many studies have extensively explored the relationship between solar eclipses and total electron content (TEC) variations. Many studies have been extensively studied over the past years on the relationship between solar eclipses and total electron content variations [1,3–5].

The total number of electrons provides an accurate reflection of the condition and dynamics of the ionosphere's F-region. By monitoring Total Electron Content (TEC), it is possible to examine the ionosphere's dynamics during a solar eclipse. Satellite data have been utilized to investigate the dynamic impacts of the ionosphere during a solar eclipse [11–13].

As a result of changes in altitude within the neutral composition of the atmosphere and variations in the rate of production with altitude,

^{*} Corresponding author at: National University of Uzbekistan, Faculty of Physics, University Street 4, Tashkent 100095, Uzbekistan. E-mail address: husan@astrin.uz (H.E. Eshkuvatov).

Table 1
GPS stations information for TEC measurements made in this research.

Station	Longitude	Latitude	Eclipse mag(Area)
MTAL, Maidantal, Tashkent, Uzbekistan	70° 38′	41° 59′	0.6119 (52%)
KIT3, Kitab, Kashkadarya, Uzbekistan	66° 53′	39° 08′	0.6545 (57%)
MADK, Maidanak, Kashkadarya, Uzbekistan	66° 53′	38° 40′	0.6668 (58%)
JFNG, Jiufeng, Fujion, China	114° 29′	30° 30′	0.9434 (92%)
LHAZ, Lhasa, China	91° 06′	29° 39′	0.9527 (94%)
BJFS, Fangshan, China	115° 53′	39° 36′	0.9663 (95%)

the plasma density in the ionosphere forms vertical layer structures known as the D, E, and F layers. These layers are governed by different physical and chemical processes and have distinct ion compositions. Various solar flares, solar eclipses, and extraterrestrial events can disrupt the physical and chemical properties of the ionospheric layers (see, e.g., [14–16]). Such distortions can modulate radio signals accordingly. The D and E layers are also reported to be associated with sporadic metal layers [17,18].

During a new moon, the Moon can pass between the Earth and the Sun, resulting in a solar eclipse. If the Moon's shadow falls on the Earth's surface, part of the solar disk will be covered or "eclipsed" by the Moon. This alignment occurs at least twice a year, allowing a portion of the Moon's shadow to fall on the Earth's surface, making the solar eclipse visible from specific locations. The TEC values used in this investigation are derived from GPS data [19–23] and are part of a study examining the ionospheric effects of solar eclipses through GPS amplitude scintillations. The Moon's shadow consists of two parts: the penumbra (semi-shadow) and the umbra, as shown in Fig. 1. Fig. 2 illustrates a map of the visibility of the annular solar eclipse on June 21, 2020.

It is well known that the effects of a solar eclipse vary depending on location, season, atmospheric region, time of occurrence, duration, and type (partial, annular, or total) of the eclipse. This topic has become increasingly attractive to the radio and ionosphere science community. In the study by [24], it was observed that the Total Electron Content (TEC) in the F-layer, derived from ground-based Global Navigation Satellite System (GNSS) receivers, experienced a significant electron density (N_e) enhancement over the continental United States (CONUS) near the first contact of the solar eclipse on August 21, 2017.

Several visible effects result from the reduction in solar radiation flux in the ionosphere during a solar eclipse, including a decrease in electron density in the E and F1 layers due to plasma transport and the dynamics of chemical reactions. The associated changes in the height of ionospheric layer boundaries and the appearance and propagation of gravity waves, along with other related phenomena during solar eclipses, have been studied (e.g., [25–30]). A solar eclipse provides a unique opportunity to study the response of the thermosphere and ionosphere to the sharp decrease in ionizing solar radiation caused by the partial occlusion of the solar disk by the Moon.

In [6], a quantitative forecast of the impact of the upcoming solar eclipse on the I–T system is described using Thermosphere–Ionosphere–Electrodynamics General Circulation Model simulations. A significant enhancement in total electron content (TEC) of approximately 2 TEC units was observed in the equatorial ionization anomaly region, even while this region remained in the eclipse's shadow. These processes lead to the formation of plasma, which interacts chemically with neutrals, disperses due to gravity and pressure gradients, and is transported by neutral winds and electric fields under the influence of the magnetic field. Based on the simulated ray propagation paths of the reflected and dispersed waves, [31] found that anomalous echoes were propagated by field-aligned irregularities (FAIs) in the E-region.

When the Moon and Earth align perfectly, an annular solar eclipse occurs, where the Moon's apparent size is smaller than that of the Sun. As a result, the Sun appears as a bright ring surrounding the dark disk of the Moon. Numerous researchers have studied the effects of solar eclipses on the ionosphere (see, e.g., [32–41]).

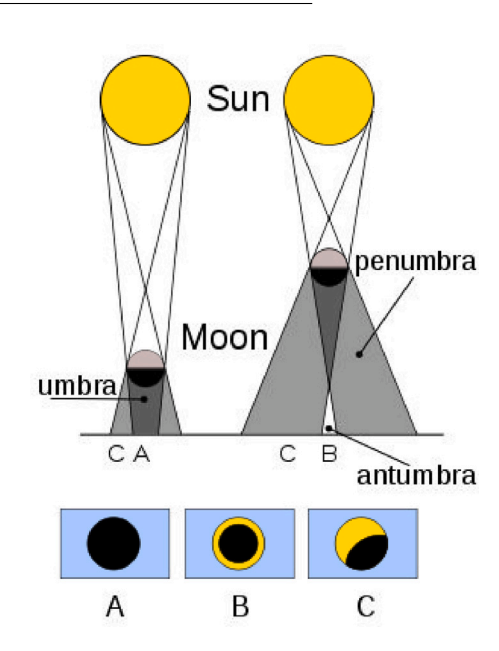


Fig. 1. Categories of solar eclipses: A is a total solar eclipse, B is an annular solar eclipse, and C is a partial solar eclipse. https://eclipse.gsfc.nasa.gov/.



Fig. 2. The annular solar eclipse that took place on June 21, 2020, as seen from around the world (https://eclipse.gsfc.nasa.gov/).

Ionospheric disturbances at low latitudes can disrupt the amplitude and phase of radio signal propagation, an effect known as scintillation. Scintillation depends on various factors, including the roughness strength and layer thickness, the satellite's zenith angle, the angle between the radiation path and Earth's magnetic field, local time, season, solar and magnetic activity, and signal frequency. Scintillation typically occurs when the Fresnel scale of the propagating radio wave matches the scale of irregularities in the ionosphere [42].

The Maidanak and Maidantal GPS stations are part of the regional research network Water in Central Asia (CAWa), coordinated by the German Research Centre for Geosciences (GFZ-Potsdam) in collaboration with the Ulugh Beg Astronomical Institute and UzHydromet,

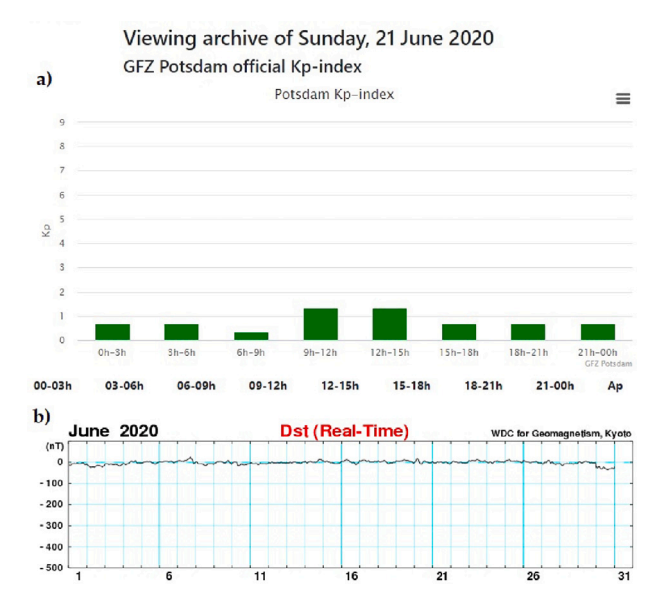


Fig. 3. Variations of (a) Kp index for 21 June 2022, (b) Dst index for the geomagnetic storms during June 2020.

Uzbekistan. Maidanak is an internationally recognized observatory known for its excellent atmospheric conditions, making it ideal for optical astronomical observations [43,44]. By studying ionospheric changes during a solar eclipse, it is possible to predict the timing of the eclipse and analyze the resulting data distortions. This paper is organized as follows: Section 2 focuses on the data and methods of analysis used (see Table 1).

The obtained results and analyses are summarized in Section 3. In Section 4, detailed explanations and discussions are given, and, finally, a summary of conclusions is provided in Section 5.

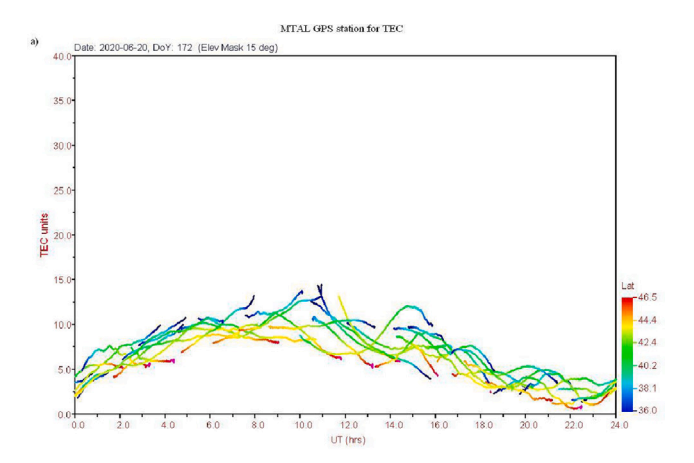
2. Data and methods

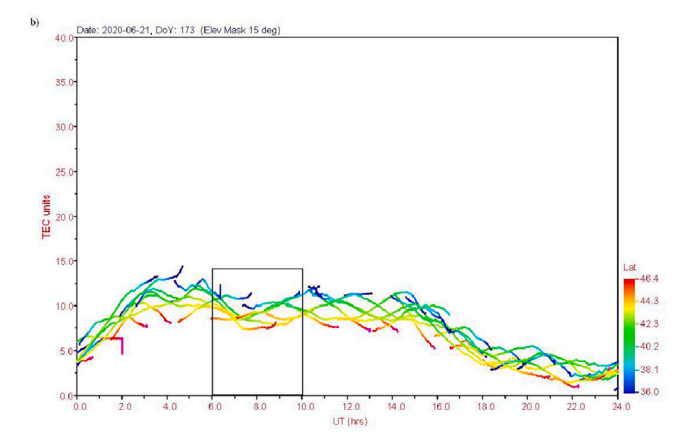
2.1. The TEC and VTEC measurements

We monitored total electron content (TEC) in the F-layer and GPS amplitude scintillations using six GPS receivers located in Uzbekistan and China. The GPS stations MADK, MTAL, KIT3, JFNG, LHAZ, and BJFS provide real-time data for calculating ionospheric parameters such as TEC and the S_4 index, using the full temporal resolution of the selected receivers. TEC is derived from the pseudo-range and carrier phase measurements at the L_1 (1.575 GHz) and L_2 (1.228 GHz) frequencies [45], along the path from the receiver to the satellite. The TEC measured along the line of sight of a satellite signal is known as slant TEC (STEC). Receiver Independent Exchange (RINEX) tracking files processed using Gopi Seemala's RINEX software (version 3.0.2) provide the required (.CMN) and (.STD) output files [46]. STEC measures the total number of free electrons in a column of unit cross-section along the path of an electromagnetic wave between a satellite and a receiver. STEC and TEC_{be} are typically obtained from dual-frequency code readings.

$$STEC = \frac{1}{40.3} \times \left(\frac{L_1^2 \times L_2^2}{L_2^2 - L_1^2}\right) \times (P_1 - P_2) + TEC_{be} , \qquad (1)$$

where P_1 (L_1) is the pseudo-range at the L_1 frequency, P_2 (L_2) is the pseudo-range at the L_2 frequency, and TEC_{be} is used to correct errors in the line of sight between different satellite-receiver pairs. Vertical TEC (VTEC) is derived by projecting the slant TEC onto the vertical line





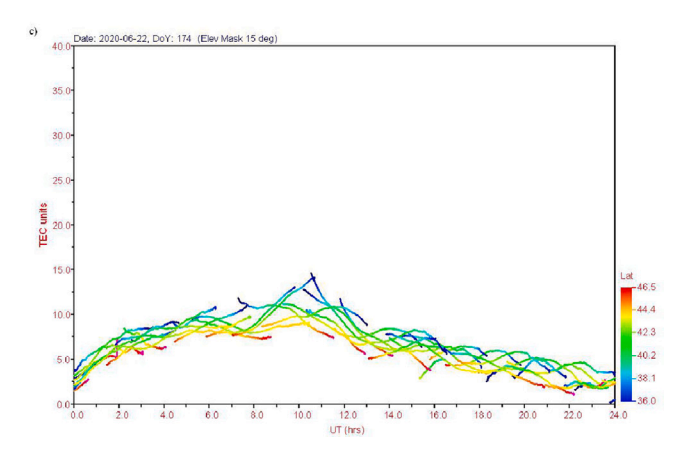


Fig. 4. Daily variation of slant TEC at MTAL GPS station on (a) 20th, (b) 21st, and (c) 22nd June 2020. The square indicates where the solar eclipse was most extreme at the MTAL GPS station in Uzbekistan. (The eclipse hours period has been indicated with the black box in column (b)).

using a thin shell model positioned 350 km above sea level, following the methodology outlined in [21,22,47–49].

$$VTEC = STEC \times \cos \left[\arcsin \left(\frac{R_e \sin z}{R_e + h_{max}} \right) \right], \tag{2}$$

where the radius of the Earth, $R_e = 6378$ km, the maximum height to the pierce point, $h_{max} = 350$ km, and z is the angle of elevation at the ground station. For a detailed analysis of the TEC response to a Solar eclipse, we have studied the variation of the absolute TEC across

the five satellite transitions. Regional TEC models were obtained using regional baseline functions to analyze the spatial distribution of TEC during a Solar eclipse. For regional modeling of TEC, we used GPS measurements collected at about 10 IGS stations using pseudo-range code and phase measurements.

2.2. Ionospheric S_4 index scintillations

Irregularly structured ionospheric regions can lead to diffraction and propagation of trans-ionosphere radio signals. When received on an antenna, these radio signals show random transient oscillations in amplitude and phase. This is called ionosphere scintillation. Ionosphere scintillation can cause problems such as signal strength loss, phase cycle slip, loss of receiver block, etc., and deteriorate the quality of satellite navigation systems. Ionosphere scintillation is a rapid oscillation of the phase or/and amplitude of a radio frequency signal that is generated when a signal passes through the F- a layer of the ionosphere. Scintillation occurs when a straight-wave radio frequency signal crosses a region of small-scale irregularities in electron density. Ionospheric scintillation is a well-known phenomenon that has been extensively studied a lot in the past, see e.g. [50]. However, large-scale prediction or modeling remains a difficult phenomenon. Scintillation occurs as a result of small-scale oscillations of the susceptibility index of the ionospheric environment, which in turn is the result of inhomogeneities. Ionospheric disturbances can affect satellite communication and navigation by causing radio signals. Scintillations are routinely measured using ground-based networks of receivers. For example, a discussion of ionospheric disturbance observations by Langmuir probes on Swarm satellites is published in the paper [51].

Inhomogeneities in the ionospheric medium are produced by a wide range of phenomena (e.g. plasma bubbles) and those responsible for scintillation occur mainly where the F-layer is located ionosphere at altitudes of 200 to 1000 km. However, the primary is typically located in zone F, which is 250 to 400 km. Electronic layer asymmetries such as sporadic-E and auroral E can also cause scintillation, but their effect on GPS signals in the L range is minimal and insignificant. Ionospheric scintillation is primarily an equatorial and high-latitude ionosphere phenomenon, although it can (and does) occur at lower intensities at all latitudes. The irregularities lead to small-scale fluctuations in the refractive index and subsequent differential diffraction (propagation) of the plane wave, which causes phase changes along the phase front of the signal. As the propagation of the signal continues after passing through the zone of disturbances, phase and amplitude scintillation develops through the interference of several scattered signals. The widely used S_4 and σ ionosphere scintillation indices show the amplitude and intensity of phase scintillation affecting GPS receivers. The four quantitative S_1 , S_2 , S_3 , S_4 indices are as follows [52]:

$$S_1 = \frac{1}{\langle I \rangle} \langle |I - \langle I \rangle| \rangle = 0.42 S_4, \tag{3}$$

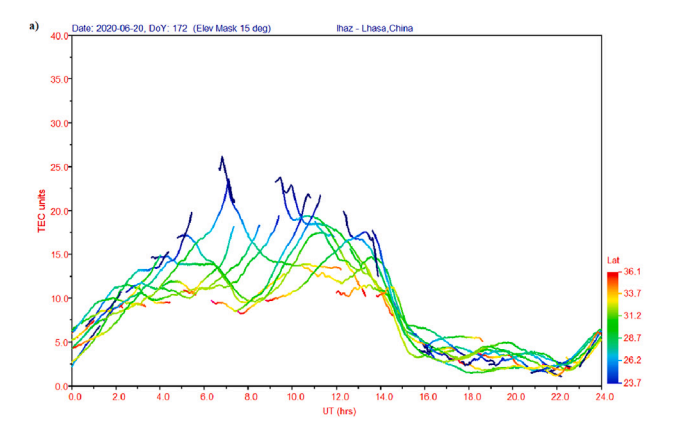
$$S_2 = \frac{1}{\langle I \rangle} \sqrt{\langle (I - \langle I \rangle)^2 \rangle} = 0.52 S_4, \tag{4}$$

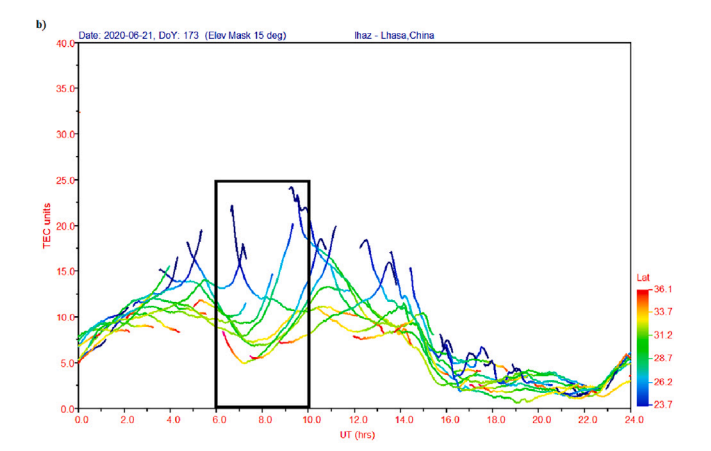
$$S_3 = \frac{1}{\langle I^2 \rangle} \langle |I^2 - \langle I^2 \rangle| \rangle = 0.73 S_4, \tag{5}$$

$$S_4 = \frac{1}{\langle I \rangle} \sqrt{\langle I^2 \rangle - \langle I \rangle^2} , \qquad (6)$$

where I is the signal intensity [53]. The index S_4 is the ratio of the departure from the norm for the signal strength to the average signal strength calculated over a period of time. S_4 is a dimensionless number with a theoretical upper limit of 1.0, commonly estimated over an interval of 60 s. There are two defined modes of amplitude scintillation: weak and strong, which roughly correspond to the type of associated scattering.

Strong scintillation is typically observed when the S_4 index exceeds 0.6, indicating significant signal propagation effects in the ionosphere.





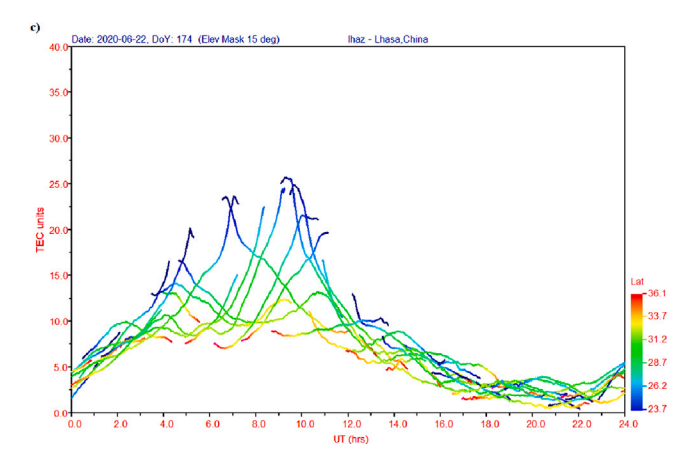


Fig. 5. Daily variation of slant TEC at LHAZ GPS station on (a) 20th, (b) 21st, and (c) 22nd June 2020. The square depicts the greatest phase of the solar eclipse at the LHAZ GPS location in China. (The eclipse hours period has been indicated with the black box in column (h))

Conversely, if the S_4 index is below 0.3, it is unlikely to have a notable impact on GPS signals. An Ionosphere Scintillation Monitor (ISM) is a specialized GPS receiver, either single or dual-frequency, designed to monitor ionospheric scintillation levels in real-time. The ISM features wide-bandwidth tracking loops that help maintain signal lock for longer periods during strong scintillation events. It samples at a rate of 50 Hz to calculate scintillation statistics, including the S_4 index and σ . While wide-bandwidth tracking enhances the receiver's ability to track signals during strong scintillation, loss of lock on one or more satellites can still occur during extreme events, necessitating signal re-acquisition.

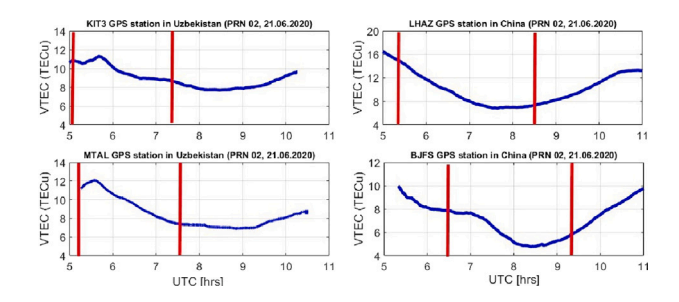


Fig. 6. Variation of vertical TEC for KIT3, MTAL, LHAZ, and BJFS stations on the 21st of June, 2020, during the solar eclipse. (The vertical red line highlights the eclipse hours). (For interpretation of the references to color in this figure legend, the reader is referred to the web version of this article.)

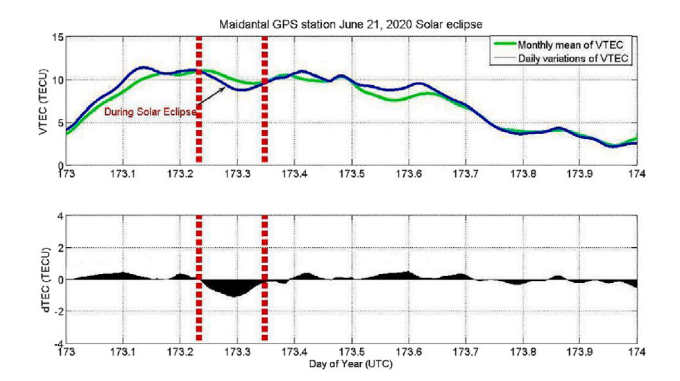


Fig. 7. The decrease of vertical and differential TEC during the Solar eclipse occurred on 21 June 2020 at the MTAL GPS station in Uzbekistan. The beginning and finish of the eclipse are shown by vertical dashed lines.

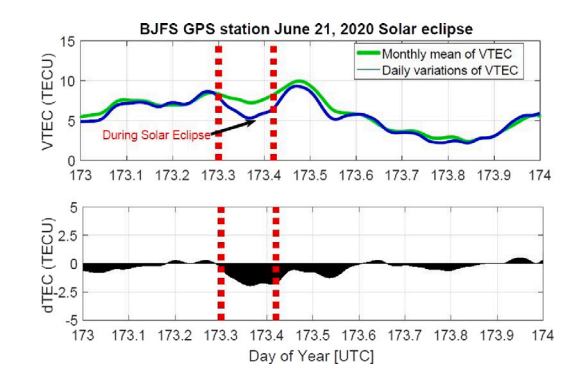


Fig. 8. The decrease of vertical and differential TEC during the Solar eclipse occurred on 21 June 2020 at the BJFS GPS station in China. The beginning and finish of the eclipse are shown by vertical dashed lines.

3. Results and analyses

To study the effects of the solar eclipse on TEC variations, a method based on daily TEC fluctuations has been employed. This approach compares data from three days following the solar eclipse to examine TEC variations at a single location. The variations of slant TEC, derived from phase measurements, for the day of, during, and after the solar eclipse along satellite passes are presented in Figs. 4 and 5. These figures show the daily slant TEC variations over the MTAL and LHAZ GPS stations on June 20th, 21st, and 22nd, 2020. The time series includes GPS measurements from all satellites over a 24-h period. The black boxes indicate the time interval corresponding to the solar eclipse's date and timing over the selected stations. These figures represent the similar behavior of slant TEC variations observed at other stations; for

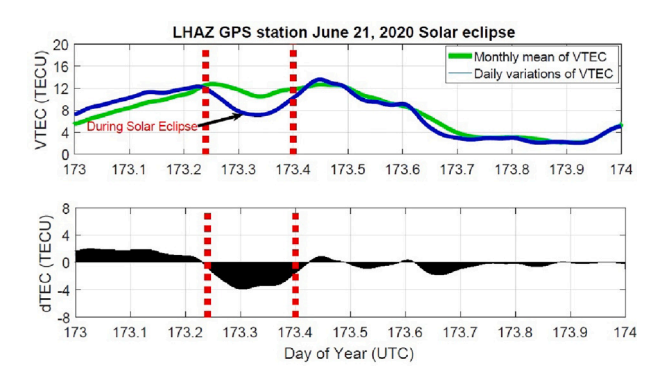


Fig. 9. The decrease of vertical and differential TEC during the Solar eclipse occurred on 21 June 2020 at the LHAZ GPS station in China. The beginning and finish of the eclipse are shown by vertical dashed lines.

example, the MADK and KIT3 data exhibit the same pattern as MTAL, shown in Fig. 4, while the data from JFNG and BJFS follow a similar trend to LHAZ, as shown in Fig. 5.

In addition, we investigate the Solar eclipse that occurred during quiet geomagnetic conditions. The indices K_p and A_p are usually lower than 3. In this study, the values of F10.7, K_p , A_p , and Dst indices are used to check the solar and geomagnetic activities. The World Data Centre Kyoto (http://wdc.kugi.kyoto-u.ac.jp) and NASA OMNI Web (https://omniweb.gsfc.nasa.gov) are where these indices are obtained. as well as on June 21, 2020, the day of the annular Solar eclipse, we queried geomagnetic data and analyzed some of these data to identify the relationship between geomagnetic data and the ionosphere. The K_p index is usually lower than 3 for 21 June, 2020 and the Dst index is usually greater than -20 nT are shown in Fig. 3a, b, respectively. [54] found that a thermosphere composition and ionospheric total electron content (TEC) variations during two geomagnetically quiet periods (maximum $K_p = 1.7$) at solar minimum.

It can be observed that the TEC values during the eclipse are lower than they would be on any other day for the same time period. Fig. 4(b) illustrates how the eclipse effect manifests as a dip that resembles a trough. at the time of the eclipse's maximum phase for each station, the TEC values reach their minimum. The minimum level of TEC persists for around 20–50 min, and then it slowly recovers during the next 2–4 h. The data of other stations behave analogously.

Fig. 6 demonstrates vertical TEC (VTEC - slant TEC reduced to zenith) for KIT3, MTAL, LHAZ, and BJFS stations during the annular Solar eclipse. The onset and finish of the eclipse are shown by red vertical lines. The TEC behavior at the other two locations is comparable to these graphs. For all of the stations, there is a considerable drop in total electron content. As may be observed during the solar eclipse the TEC depression around 8 Universal Time (UT) is recognized for all satellites (Fig. 5 - columns (b)). Each station has a distinct period when the TEC value is at its lowest relative to the eclipse's greatest phase, and each satellite has a different amount of TEC depression. A decrease in the total electron content with elevation angles was observed in several satellites at the MADK GPS station during the annular Solar eclipse, i.e., PRN 02, PRN 06, PRN 12, and PRN 25 are presented in Fig. 11 and Kitab GPS station satellites were observed, i.e. PRN 02, PRN 06, PRN 12, PRN 25 are presented in Fig. 12. LHAZ GPS station several satellites were observed, i.e. PRN 02, PRN 06, PRN 12, and PRN 25 are presented in Fig. 13. BJFS GPS station several satellites were observed, i.e. PRN 02, PRN 04, PRN 06, and PRN 25 are presented in Fig. 14. Variations of TEC and S4 indices were in observed several satellites at the MTAL GPS station during the annular Solar eclipse, i.e., PRN 02 and PRN 06 are presented in Fig. 19 and MADK GSP station during the annular Solar eclipse, i.e., PRN 02 and PRN 06 are presented in Fig. 20

Table 2
Ionospheric Scintillation Index S4 measurements for GPS stations during continuous three days.

GPS stations (2 h)	S4aver	S4std	S4medi	S4min	S4max	Eclipse mag (Area)
MTAL (June 20, 2020)	0.0880	0.0957	0.0620	0.0190	0.7830	
MTAL (June 21, 2020)	0.0858	0.0890	0.0570	0.0240	0.7160	0.6119 (52%)
MTAL (June 22, 2020)	0.0965	0.0902	0.0820	0.0170	0.4610	
BJFS (June 20, 2020)	0.0738	0.0289	0.0690	0.0260	0.1980	
BJFS (June 21, 2020)	0.0646	0.0123	0.0680	0.0190	0.2150	0.9663 (95%)
BJFS (June 22, 2020)	0.0753	0.0381	0.0670	0.0150	0.3250	

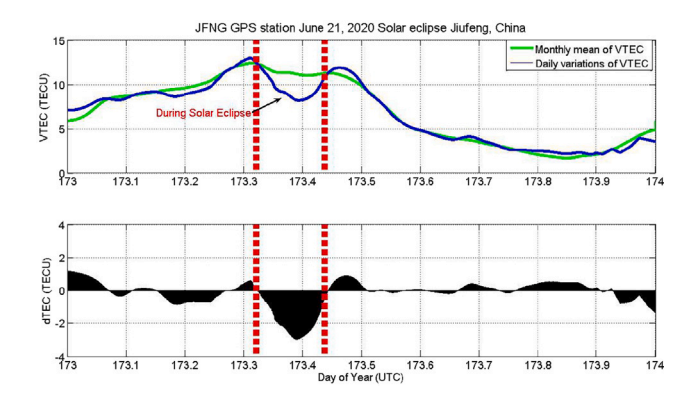


Fig. 10. A decrease of vertical and differential TEC during the Solar eclipse occurred on 21 June 2020 at the JFNG GPS station in China. The beginning and finish of the eclipse are shown by vertical dashed lines.

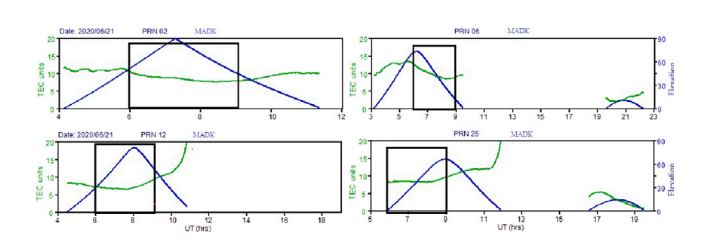


Fig. 11. Variation of TEC with elevation angels along satellite passes PRN 02, PRN 06, PRN 12, and PRN 25 rows for MADK GPS station on June 21, 2020, the day of the solar eclipse. (The black box highlights the from 06:00 until after 09:00 UT hours.)

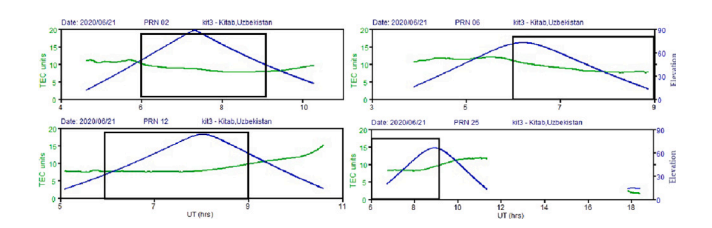


Fig. 12. Variation of TEC with elevation angels along satellite passes PRN 02, PRN 06, PRN 12, and PRN 25 rows for KIT3 GPS station on June 21, 2020, the day of the solar eclipse. (The black box highlights the from 06:00 until after 09:00 UT hours).

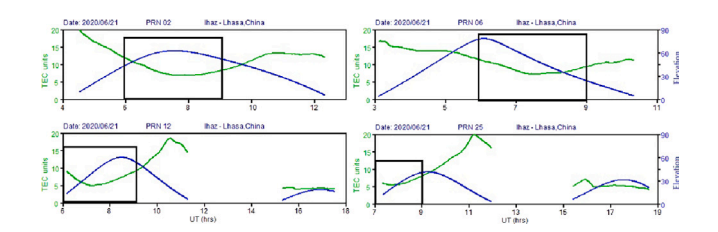


Fig. 13. Variation of TEC with elevation angels along satellite passes PRN 02, PRN 06, PRN 12, and PRN 25 rows for LHAZ GPS station on June 21, 2020, the day of the solar eclipse. (The black box highlights the from 06:00 until after 09:00 UT hours).

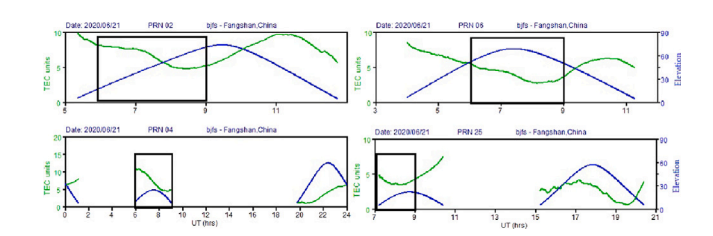


Fig. 14. Variation of TEC with elevation angels along satellite passes PRN 02, PRN 04, PRN 06, and PRN 25 rows for BJFS GPS station on June 21, 2020, the day of the solar eclipse. (The black box highlights the from 06:00 until after 09:00 UT hours).

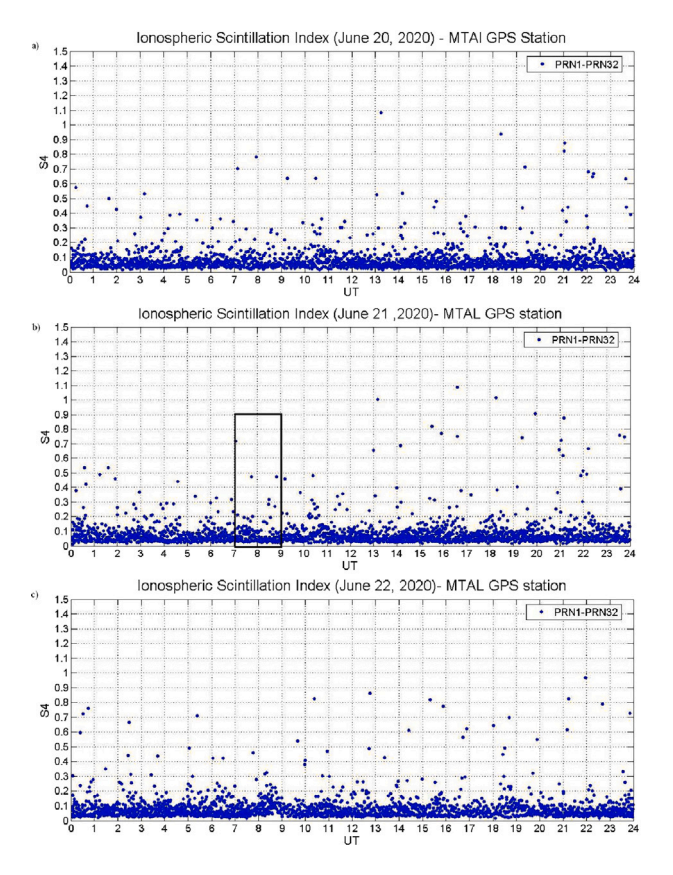


Fig. 15. Diurnal variation of the amplitude scintillation index S_4 values based on data of MTAL station at (a) one day before the eclipse (b) the day of solar eclipse occurrence and (c) one day after the event. (The eclipse hours period has been indicated with the black box).

4. Discussion

Modern ionospheric research is greatly aided by the ionosphere and the idea of ionospheric development that has been developed in the literature. The ionospheric steady state is formed on the combined action of the light chemistry, thermodynamics, kinetics, electrodynamics, and

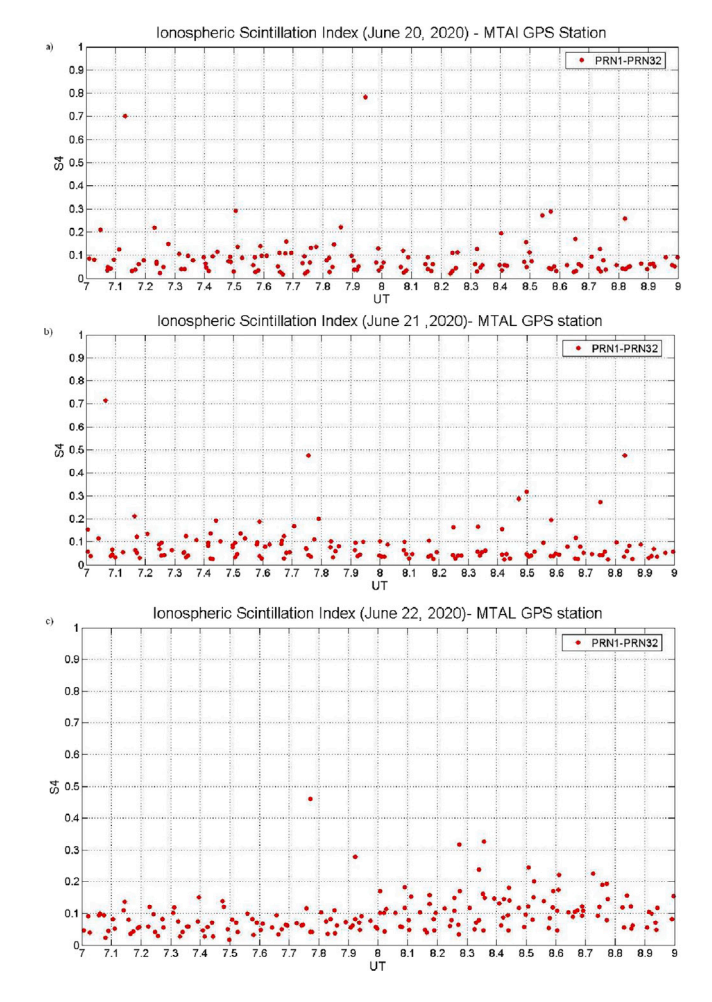


Fig. 16. Variation of the amplitude scintillation index S_4 values based on data of MTAl station during continuous two hours.

other processes [55,56]. It has not only a complex spatial distribution structure but also has time-varying characteristics with different time scales which are controlled by multiple mechanisms. In the beginning pioneering stage of active studies of the ionosphere, an observed ionospheric phenomenon that could not be explained by the Chapman theory of solar photoionization of the neutral atmosphere [57] was often called anomalous.

Later it was realized that at altitudes (heights of F region) where these anomalies were observed, the plasma was no longer in photochemical equilibrium and that transport processes due to diffusion, neutral winds, and electromagnetic drifts played an important role [58, 59], and deviations from the simple Chapman theory could be expected. The F region is usually divided into three subregions. The lowest region, where photochemistry dominates, is called the F1 region. The topside ionosphere is the region in the upper F region where diffusion dominates and where there is a change from chemical to diffusion dominance, also known as the F2 region. In the F1 area, the photochemistry is simplified because only one ion (O^+) dominates. The important reactions are photoionization of neutral atomic oxygen and loss in reactions with N_2 and O_2 .

The Figs. 7, 8, 9 and 10 show the vertical and differential TEC variations in 21 June 2020 above MTAL, BJFS, LHAZ and JFNG stations, respectively. Vertical red lines denote the duration of the Solar eclipse i.e. beginning and end. Differential TEC is obtained by subtracting monthly averaged diurnal vertical TEC from the values of observed

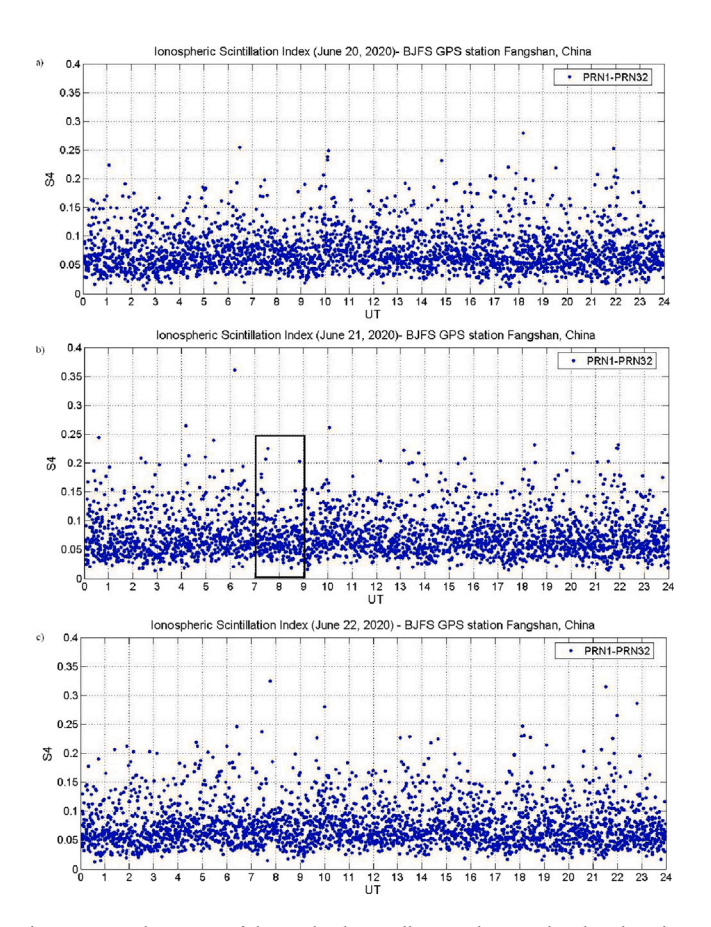


Fig. 17. Diurnal variation of the amplitude scintillation index S_4 values based on data of BJFS station at (a) one day before (b) the day of the solar eclipse occurrence and (c) one day after the event. (The eclipse hours period has been indicated in the black box).

vertical TEC at each epoch. Vertical and differential TEC fluctuations show that differential TEC decreases during the solar eclipse.

Figs. 15 and 17 demonstrate this, as can be seen. Ionospheric Scintillation Index S4 values show a slight reduction during the occurrence of total solar eclipse, i.e. on 21st of June from around 07:00 until after 09:00 UT at the stations MTAL (Fig. 16.) and BJFS (Fig. 18).

5. Conclusions

Central and South-East Asia were able to see the annular solar eclipse on June 21, 2020, which offered a great opportunity to study ionospheric behavior under eclipse conditions.

In order to examine the ionospheric reaction to this event, GPS measurements over Uzbekistan and China on the eclipse's day, the day before it occurred, and the day after it were processed. When a solar eclipse occurs, variations in the S_4 values, which represent variations in the occurrence of ionospheric scintillation, have been examined (see Table 2). Although the first two factors were carefully studied by a number of writers, ionospheric scintillation caused by solar eclipses has only recently been studied utilizing stations that are now located in Central and Southeast Asia. In terms of TEC values, the results at various stations and for each signal path from a satellite to a receiver showed a drop between 1 and 5 TECU during the total solar eclipse, which fits earlier research as well as theoretical assumptions [2,60].

The amplitude scintillation index S_4 values of data based on station MTAL during the annular solar eclipse hours (values within the black box in Fig. 15(b)) have been reduced by about 6.94% when compared

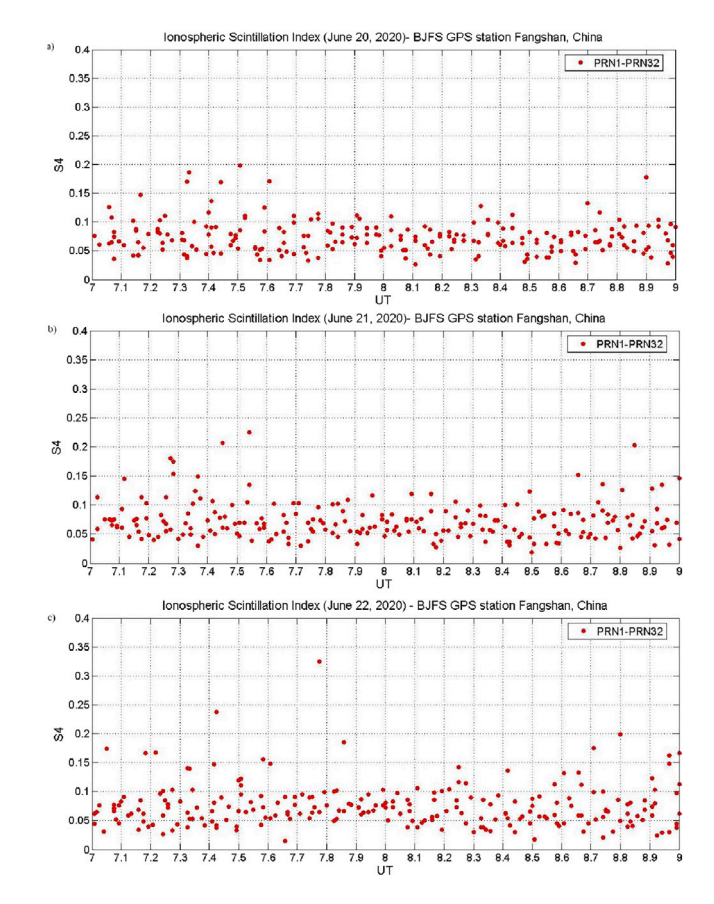


Fig. 18. Variation of the amplitude scintillation index S_4 values based on data of BJFS station during continuous two hours.

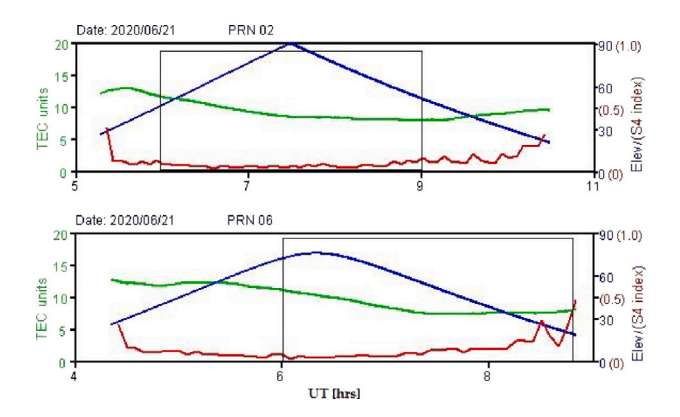


Fig. 19. Variations of TEC and S4 indices along satellite passes (PRN 02 and PRN 06 rows, respectively) for MTAL GPS station on June 21, 2020, the day of the solar eclipse. (The black box highlights the from 06:00 until after 09:00 UT hours).

with similar time on the day before and the day after the annular solar eclipse. A similar comparison is made using the data from station BJFS, which revealed a reduction of 13.34% in the values of the amplitude scintillation index S_4 (values within the black box in Fig. 17(b)). It can be inferred that the ionospheric scintillation was significantly reduced in two GPS stations during the occurrence of the annular solar eclipse because the amplitude scintillation index S_4 values are directly connected to the occurrence of ionospheric scintillation.

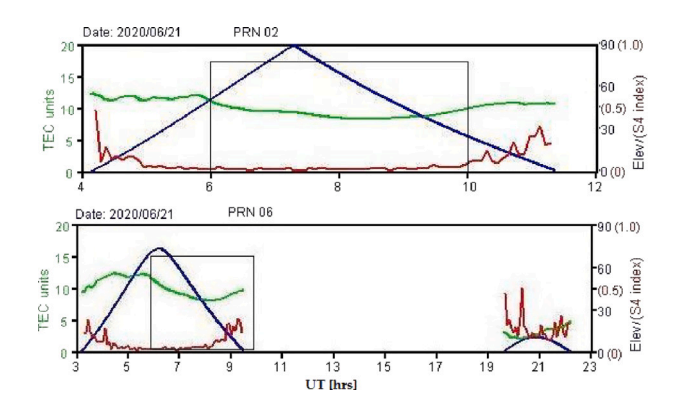


Fig. 20. Variations of TEC and S4 indices along satellite passes (PRN 02 and PRN 06 rows, respectively) for MADK GPS station on June 21, 2020, during the solar eclipse. (The black box highlights the from 06:00 until after 10:00 UT hours).

CRediT authorship contribution statement

H.E. Eshkuvatov: Writing – original draft, Investigation, Formal analysis, Data curation, Conceptualization.

Declaration of competing interest

The authors declare that they have no known competing financial interests or personal relationships that could have appeared to influence the work reported in this paper.

Acknowledgments

This work was financially supported by the Fundamental Fund (FF68) of the Thailand Science Research and Innovation Fund (Grant Number: RE-KRIS/FF68/84)

Data availability

The data that has been used is confidential.

References

- E. Şentürk, M. Arqim Adil, M. Saqib, Ionospheric total electron content response to annular solar eclipse on june 21, 2020, Adv. Space Res. 67 (6) (2021) 1937–1947, http://dx.doi.org/10.1016/j.asr.2020.12.024.
- [2] Mohamad Mohdi Alizadeh, Harald Schuh, Saeed Zare, Sahar Sobhkhiz-Miandehi, lung-Chin Tsai, Remote sensing ionospheric variations due to total solar eclipse, using GNSS observations, Geod. Geodyn. 11 (2020) 202–210.
- [3] F. Huang, Q. Li, X. Shen, C. Xiong, R. Yan, S. Zhang, W. Wang, E. Aa, J. Zhong, T. Dang, J. Lei, Ionospheric responses at low latitudes to the annular solar eclipse on 21 2020, J. Geophys. Res.: Space Phys. 125 (10) (2020) http://dx.doi.org/10.1029/2020ja028483.
- [4] J. Wang, Y. Sun, T. Yu, Y. Wang, T. Mao, H. Yang, C. Xia, X. Yan, N. Yang, G. Huang, Yifan qi, Convergence effects on the ionosphere during and after the annular solar eclipse on 21 2020, J. Geophys. Res.: Space Phys. 127 (9) (2022) http://dx.doi.org/10.1029/2022ja030471.
- [5] E. Aa, S.R. Zhang, H. Shen, S. Liu, J. Li, Local and conjugate ionospheric total electron content variation during the 21 june 2020 solar eclipse, Adv. Space Res. 68 (8) (2021) 3435–3454, http://dx.doi.org/10.1016/j.asr.2021.06.015.
- [6] T. Dang, J.H. Lei, W.B. Wang, M.D. Yan, D.X. Ren, F.Q. Huang, Prediction of the thermospheric and ionospheric responses to the 21 june 2020 annular solar eclipse, Earth Planet. Phys. 4 (3) (2020) 231–237, http://dx.doi.org/10.26464/ epp2020032.
- [7] M.N. Shrivastava, A.K. Maurya, K.N. Kumar, Ionospheric perturbation during the south American total solar eclipse on 14th december 2020 revealed with the Chilean GPS eyeball, Sci Rep 11 (2021) 20324, http://dx.doi.org/10.1038/ s41598-021-98727-w.
- [8] A.K. Maurya, D.V. Phanikumar, R. Singh, S. Kumar, B. Veenadhari, Y.S. Kwak, A. Kumar, A.K. Singh, K. Niranjan Kumar, Low-mid latitudedregionionospheric perturbations associated with 22 july 2009 total solar eclipse: Wave-like signatures inferred from VLF observations, J. Geophys. Res. Space Phys. 119 (2014) 8512–8523, http://dx.doi.org/10.1002/2013JA019521.

- [9] G. Chimonas, Internal gravity-wave motions induced in the earth's atmosphere by a solar eclipse, J. Geophys. Res. 75 (28) (1970) 5545–5551.
- [10] R.A. Antonia, A.J. Chambers, D. Phong-Anant, S. Rajagopalan, K.R. Sreenivasan, Response of atmospheric surface layer turbulence to a partial solar eclipse, J. Geophys. Res. 84 (C4) (1979) 1689–1692.
- [11] E.A. Cohen, The study of the effect of solar eclipse on the ionosphere based on satellite beacon observation, Radio Sci. 19 (3) (1984) 769–777.
- [12] J.E. Salah, W.L. Oliver, J.C. Foster, J.M. Holt, Observation of the may 30, 1984, annular solar eclipse at Millstone Hill, J. Geophys. Res. 91 (A2) (1986) 1651–1660.
- [13] K.C. Yeh, D.C. Yu, K.H. Lin, C.H. Liu, C.R. Huang, et al., Ionospheric response to a solar eclipse in the equatorial anomaly region, Terr. Atmos. Ocean. Sci. 8 (2) (1992) 165–178.
- [14] M.A. Clilverd, C.J. Rodger, N.R. Thomson, Total solar eclipse effects on VLF signals: Observations and modeling, Radio Sci. 36 (2001) 773.
- [15] S.K. Chakrabarti, S.K. Mondal, S. Sasmal, VLF signals in summer and winter in the Indian sub-continent using multi-station campaigns, Indian J. Phys. 86 (2012) 323–334.
- [16] U.S. Inan, N.G. Lehtinen, R.C. Moore, K. Hurley, S. Boggs, D.M. Smith, G.J. Fishman, Massive disturbance of the daytime lower ionosphere by the giant g-ray flare from magnetar SGR 1806-20, Geophys. Res. Lett. 34 (2007) L08103.
- [17] T. Yuan, J. Wang, X. Cai, J. Sojka, D. Rice, J. Oberheide, N. Criddle, Investigation of the seasonal and local time variations of the high-altitude sporadic Na layer (Nas) formation and the associated midlatitude descending E layer (Es) in the lower E region, J. Geophys. Res. Space Phys. 119 (2014) 5985–5999.
- [18] R.W. Schunk, A.F. Nagy, Ionospheres: Physics, Plasma Physics, and Chemistry, second ed., Cambridge University Press, Cambridge, UK, http://dx.doi.org/10. 1017/CBO9780511635342.2009.
- [19] S.R. Tojiev, B.J. Ahmedov, Y.A. Tillayev, H.E. Eshkuvatov, Ionospheric anomalies of local earthquakes detected by GPS TEC measurements using data from Tashkent and Kitab stations, Adv. Space Res. 52 (2013) 1146–1154.
- [20] S.R. Tojiev, B.J. Ahmedov, H.E. Eshkuvatov, Ionospheric precursors of earth-quakes recorded by VLF receiver at Tashkent IHY station, Adv. Space Res. 54 (2014) 628-643.
- [21] S.R. Tojiev, V.S. Morozova, B.J. Ahmedov, H.E. Eshkuvatov, Electromagnetic Studies of Ionospheric and Magnetospheric Perturbations Associated with the Earth, Atmospheric and Astrophysical Phenomena, Mathematical Physics, World Scientific, 2012, pp. 254–278.
- [22] H.E. Eshkuvatov, B.J. Ahmedov, Y.A. Tillayev, M. Arslan Tariq, Libo Liu, M. Ali Shah, Ionospheric precursors of strong earthquakes observed using six GNSS stations data during five continuous years (2011-15), Geod. Geodyn. 14 (1) (2023) 65–79.
- [23] H. Eshkuvatov, B. Ahmedov, M. Shah, et al., Exploring electromagnetic wave propagation through the ionosphere over seismic active zones, Pure Appl. Geophys. (2024) http://dx.doi.org/10.1007/s00024-024-03532-x.
- [24] Z. Tian, Y. Sui, S. Zhu, Y.Y. Sun, Enhancement of electron density in the ionospheric F2 layer near the first contact of the total solar eclipse on 21 august 2017, Earth Space Sci. 9 (2022) e2021EA002016, http://dx.doi.org/10.1029/ 2021EA002016.
- [25] S. Kumar, A.K. Singh, Changes in total electron content (TEC) during the annular solar eclipse of 15 january 2010, Adv. Space Res. 49 (2012) 75–82.
- [26] P. Galav, S. Sharma, R. Pandey, Study of simultaneous penetration of electric fields and variation of total electron content in the day and night sectors during the geomagnetic storm of 23 may 2002, J. Geophys. Res. 116 (2011) A12324, http://dx.doi.org/10.1029/2011JA017002.
- [27] P.R. Jayakrishnan, C.A. Babu, P. Sivaprasad, Drastic variation in surface boundary layer parameters over cochin, during the annular solar eclipse: analysis using anemometer data, J. Atmos. Solar- Terr. Phys. 94 (2013) 49–53, http://dx.doi.org/10.1016/j.jastp.2012.12.019.
- [28] S. Sharma, N. Dashora, P. Galav, R. Pandey, Total solar eclipse of july 22, 2009: Its impact on the total electron content and ionospheric electron density in the Indian zone, J. Atmos. Solar- Terr. Phys. 72 (2010) 1387–1392.
- [29] T. Farges, A. Pichon, E. Le Blanc, S. Perez, B. Alcoverro, Response of the lower atmosphere and ionosphere to the eclipse of august 11, 1999, J. Atmos. Solar-Terr. Phys. 65 (2003) 717–726, http://dx.doi.org/10.1016/S1364-6826(03)00078-6.
- [30] F. Ding, et al., GPS TEC response to the 22 july 2009 total solar eclipse in east Asia, J. Geophys. Res. 115 (2010) A07308, http://dx.doi.org/10.1029/ 2009JA015113.
- [31] L. Qiao, G. Chen, W. Gong, X. Cai, E. Liu, M. Su, X. Teng, Z. Qiu, H. Song, E-region field- aligned irregularities in the middle of a solar eclipse observed by a bistatic radar, Remote. Sens. 14 (2022) 392, http://dx.doi.org/10.3390/ rs14020392.
- [32] L. Baran, I. Ephishov, I. Shagimuratov, V. Ivanov, A. Lagovsky, The response of the ionospheric total electron content to the solar eclipse on august 11, 1999, Adv. Space Res. 31 (4) (2003) 989–994.
- [33] J. Ratcliffe, A survey of solar eclipses and the ionosphere. Solar eclipses and the ionosphere, J. Atmos. Terr. Phys. 6 (Special suppl) (1956) 1–13.
- [34] H. Rishbeth, Solar eclipses and ionospheric theory, Space Sci. Rev. 8 (4) (1968) 543–554.

- [35] E. Afraimovich, K. Palamartchouk, N. Perevalova, V. Chernukhov, A. Lukhnev, V. Zalutsky, Ionospheric effects of the solar eclipse of march 9, 1997, as deduced from GPS data, Geophys. Res. Lett. 25 (4) (1998) 465–468.
- [36] J.A. Klobuchar, H. Whitney, Ionospheric electron content measurements during a solar eclipse, J. Geophys. Res. 70 (5) (1965) 1254–1257.
- [37] S. Kumar, A. Singh, R. Singh, Ionospheric response to total solar eclipse of 22 july 2009 in different Indian regions, Ann. Geophys. 31 (2013) 1549–1558.
- [38] T. Farges, J. Jodogne, R. Bamford, Y. Le Roux, F. Gauthier, P. Vila, D. Altadill, J. Sole, G. Miro, Disturbances of the western European ionosphere during the total solar eclipse of 11 august 1999 measured by a wide ionosonde and radar network, J. Atmos. Sol. Terr. Phys. 63 (9) (2001) 915–924.
- [39] A.J. Coster, L. Goncharenko, S.R. Zhang, P.J. Erickson, W. Rideout, J. Vierinen, GNSS observations of ionospheric variations during the 21 august 2017 solar eclipse, Geophys. Res. Lett. 44 (24) (2017) 12,041–112,048.
- [40] I. Cherniak, I. Zakharenkova, Ionospheric total electron content response to the great American solar eclipse of 21 august 2017, Geophys. Res. Lett. 45 (3) (2018) 1199–1208.
- [41] J.E. Salah, W.L. Oliver, J.C. Foster, J.M. Holt, Observation of the may 30, 1984, annular solar eclipse at Millstone Hill, J. Geophys. Res. 91 (A2) (1986) 1651–1660.
- [42] B.H. Briggs, I.A. Parkin, On the variation of radio star and satellite scintillations with zenith angle, J. Atmos. Terr. Phys. 25 (6) (1963) 339–366.
- [43] Y. Tillayev, A. Azimov, A. Hafizov, Astronomical seeing at maidanak observatory during the year 2018, Galaxies 2021 (9) (2021) 38, http://dx.doi.org/10.3390/ galaxies9020038.
- [44] A.Y. Shikhovtsev, P.G. Kovadlo, E.A. Kopylov, M.A. Ibrahimov, S.A. Ehgamberdiev, Y.A. Tillayev, Energy spectra of atmospheric turbulence for calculating C2n parameter. I. Maidanak and suffa observatories in Uzbekistan, Atmosphere 2021 (12) (2021) 1614, http://dx.doi.org/10.3390/atmos12121614.
- [45] L.B. Theodore, M.K. Paul, Simultaneous global positioning system observations of equatorial scintillations and total electron content fluctuations, J. Geophys. Res. 104 (A10) (1999) 22553–22565.
- [46] G.K. Seemala, C.E. Valladares, Statistics of total electron content depletions observed over the southern American continent for the year 2008, Radio Sci. 46 (2011) RS5019, http://dx.doi.org/10.1029/2011RS004722.
- [47] J.A. Klobuchar, Design and Characteristics of the GPS Ionospheric Time Delay Algorithm for Single Frequency Users, Institute of Electrical and Electronics Engineers, 1986, pp. 280–286.
- [48] B.J. Ahmedov, S.R. Tojiev, H.E. Eshkuvatov, Total electron content (TEC) extraction using Kitab and Tashkent GPS stations, Uzb. J. Phys. 6 (2016) 361–366.
- [49] B.J. Ahmedov, S.R. Tojiev, H.E. Eshkuvatov, Low radiofrequency radiation in the D-layer of the ionosphere and possibility of their registration on Tashkent VLF station, Uzb. J. Phys. 17 (6) (2015) 339–350.
- [50] K.C. Yeh, C.-H. Liu, Radio wave scintillations in the ionosphere, IEEE Proc. 70 (1982) 324–360, http://dx.doi.org/10.1109/proc.1982.12313.
- [51] S. Aol, S. Buchert, E. Jurua, Ionospheric irregularities and scintillations: a direct comparison of in situ density observations with ground-based L-band receivers, Earth Planets Space 72 (2020) 164, http://dx.doi.org/10.1186/s40623-020.01394 z.
- [52] RBJ. Streets, Variation of radio star and satellite scintillations with sunspot number and geomagnetic latitude, J. Can. Soc. Explor. Geophys. 5 (1969) 35–52.
- [53] E.J. Fremouw, R.L. Leadabrand, R.C. Livingstone, M.D. Cousin, C.L. Rino, B.C. Fair, R.A. Long, Early results from the DNA wideband satellite experiment -complex signal analysis. Radio Sci. 13 (1) (1978) 167–187.
- [54] X. Cai, A.G. Burns, W. Wang, L. Qian, N. Pedatella, A. Coster, et al., Variations in thermosphere composition and ionosphere total electron content under geomagnetically quiet conditions at solar-minimum, Geophys. Res. Lett. 48 (2021) e2021GL093300, http://dx.doi.org/10.1029/2021GL093300.
- [55] C. Xiong, H. Lühr, Y. Yamazaki, An opposite response of the low-latitude ionosphere at Asian and American sectors during storm recovery phases: Drivers from below or above, J. Geophys. Res.: Space Phys. 124 (2019) 6266–6280, http://dx.doi.org/10.1029/2019JA026917.
- [56] X. Wan, C. Xiong, S. Gao, et al., The nighttime ionospheric response and occurrence of equatorial plasma irregularities during geomagnetic storms: a case study, Satell. Navig. 2 (2021) 23, http://dx.doi.org/10.1186/s43020-021-00055-x
- [57] S. Chapman, The absorption and dissociative or ionizing effect of monochromatic radiation in an atmosphere on a rotating earth, Proc. Phys. Soc. 43 (1931) 26–45.
- [58] W.B. Hanson, R.J. Moffett, Lonization transport effects in the equatorial F region, J. Geophys. Res. 71 (23) (1966) 5559–5572, http://dx.doi.org/10.1029/ J7071i023p05559.
- [59] H. Rishbeth, The effect of winds on the ionospheric F2-peak, J. Atmos. Terr. Phys. 29 (1967) 225–238.
- [60] Y. Jiao, Y. Morton, S. Taylor, Comparative studies of high-latitude and equatorial ionospheric scintillation characteristics of GPS signals, in: 2014 IEEE/ION Position, Location and Navigation Symposium-PLANS, 2014, pp. 37–42.